ADVANCED MATERIALS TECHNOLOGIES

Supporting Information

for *Adv. Mater. Technol.*, DOI: 10.1002/admt.202000282

Analytical Study of Solution-Processed Tin Oxide as Electron Transport Layer in Printed Perovskite Solar Cells

*Valentina Rohnacher, Florian Ullrich, Helge Eggers, Fabian Schackmar, Sebastian Hell, Adriana Salazar, Christian Huck, Gerardo Hernandez-Sosa, Ulrich W. Paetzold, Wolfram Jaegermann, and Annemarie Pucci**

Supporting Information

Analytical Study of Solution-Processed Tin Oxide as Electron Transport Layer in Printed Perovskite Solar Cells

*Valentina Rohnacher, Florian Ullrich, Helge Eggers, Fabian Schackmar, Sebastian Hell, Adriana Salazar, Christian Huck, Gerardo Hernandez-Sosa, Ulrich W. Paetzold, Wolfram Jaegermann, Annemarie Pucci**

AUTHOR INFORMATION

Corresponding author

*A.P.: pucci@kip.uni-heidelberg.de

Outline:

1.SNOM Characterization

Scattering-type SNOM measurements in the infrared were carried out using a Neaspec GmbH SNOM. A platinum iridium coated AFM tip (Neaspec nano-FTIR-probe) operated in tapping mode (ω=231kHz) was illuminated with a broadband (λ=5-10µm) IR laser beam. Due to the interaction between the tip and the sample, light containing near-field information is scattered back into the far-field and is detected with an LN2 cooled MCT detector. White-light images together with topography were recorded with the interferometer at its center position. In order to remove the background, the data was analyzed at the second harmonic of the tip oscillation frequency. An area of 2x2µm was raster-scanned with a resolution of 200x200 pixels and an integration time of 5ms per pixel.

The scattering scanning-nearfield-optical microscopy (sSNOM) measurement (in the infrared) of a SnO_x thin film prepared with ethanol as solvent is shown in Figure S1. The optical contrast shows clearly the different composition between the islands (red regions) and the substrate (yellow regions). A reason could be that the islands are $SnCl_2$ remains from the precursor solution. Ambient ethanol contains residual water and $SnCl_2$ hardly solves in water. While spin-coating ethanol should evaporate faster than water, so $SnCl_2$ crystallize may form such islands in the film.

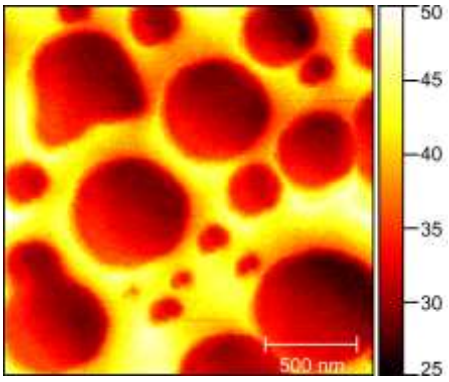

Figure S1. Optical contrast measured by infrared scattering SNOM of a $sSnO_x$ thin film from ethanol-based precursor solution, which was annealed at 200 °C. A broadband light source (5 µm to 10 µm) was used.

2. IR Analysis

2.1 Dielectric Function Model of SnO_2

The measured angle-resolved transmission spectra of $sSnO_x$ in the far infrared range was modelled using the commercially available software package SCOUT (W.Theiss[1]). The simulated layer stack consisted of a 1 mm thick Si substrate (dielectric function described elsewhere[2]) and the SnO_x film on top. The film thicknesses of the SnO_x layer and the dielectric background was determined by UV-Vis ellipsometry. For the optical model fit we used Gervais oscillators. Strong oscillators, as they occur in the far infrared range, can be described with the Gervais model[3] which allow different damping coefficients for LO and TO phonons. The dielectric function $\varepsilon(\omega)$ for Gervais oscillators is obtained as follows

$$\varepsilon(\omega) = \varepsilon_\infty \prod_j \frac{\Omega_{jLO}^2 - \omega^2 + i\gamma_{jLO}\omega}{\Omega_{jTO}^2 - \omega^2 + i\gamma_{jTO}\omega} \quad (1)$$

where Ω and γ represent the frequencies and damping of the TO and LO optical modes. ε_∞ is the high frequency dielectric constant. A fit of the Gervais oscillator was performed simultaneously on the spectra measured at 10° and 60° AOI. The results are shown in **Table S1 and Figure 2.**

Table S1. Optical mode parameters at room temperature for SnO_x thin films annealed at different temperatures. Frequencies and damping are in cm^{-1}. The values for the cassiterite are taken from Brehat et al.[4]

Sample		Ω_{jTO}	γ_{jTO}	Ω_{jLO}	γ_{jLO}
130 °C	1	258.9	136.4	272.3	113.7
	2	334.2	94.3	350.3	65.0
	3	433.4	443.3	595.5	101.0
	4	569.7	147.7	673.3	1089.0
180 °C	1	297.2	70.2	292.8	69.0
	2	337.2	199.6	355.4	96.4
	3	490.7	376.4	598.7	81.3
	4	594.6	106.6	714.2	311.2
200 °C	1	313.5	70.3	308.2	77.8
	2	327.0	212.8	351.6	94.6

	3	485.1	341.4	603.6	74.4
	4	599.4	102	718.8	303.8
250 °C	1	316.7	60.5	316.3	63.7
	2	372.1	227.3	361.9	97.5
	3	459.2	413.2	592.4	57.6
	4	587.7	67.7	708.7	212.9
400 °C	1	253.6	1.6	258.8	6.0
	2	288.1	82.1	351.2	39.2
	3	449.6	141.4	606.6	291.3
	4	578.0	86.9	621.5	230.2
Cassiterite[4]	1	244.0	12	273.0	10.0
	2	288.0	12	364.5	13.5
	3	430.0	270	480.0	330.0
	4	613.0	32	760.0	27.0

2.2. IRRAS of solution-processed tin oxide on ITO

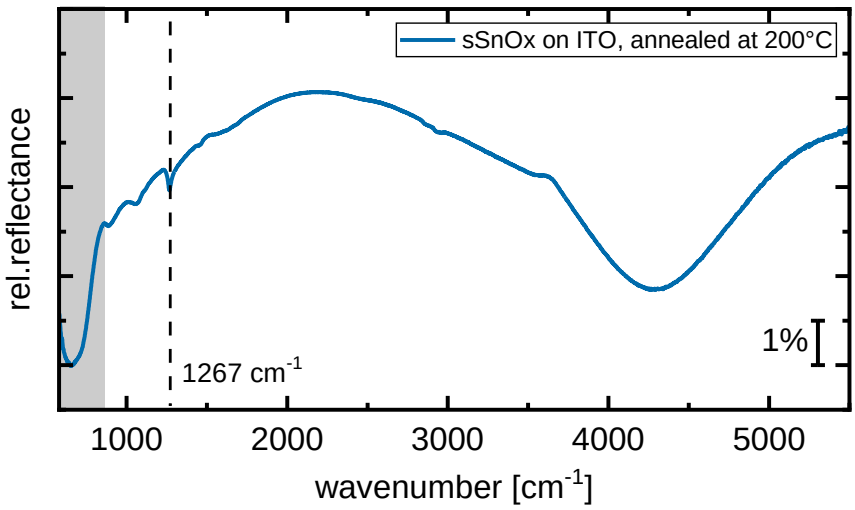

Figure S2. Infrared reflection-absorption spectra (IRRAS) in the mid infrared range of tin oxide layer prepared from precursor solution with ethanol as solvent ($SnCl_2 \cdot 2\ H_2O$) on ITO/glass and annealed at 200 °C for 60 min. The angle of incident of the p-polarized light was 75° towards the surface normal and the sample compartment was flushed with nitrogen during the measurement. At 1267 cm^{-1} the LO mode of glass substrate is visible. In the grey marked region the phonon mode of SnO_x appears.

2.3. Comparison between ethanol and methoxyethanol for the precursor solution

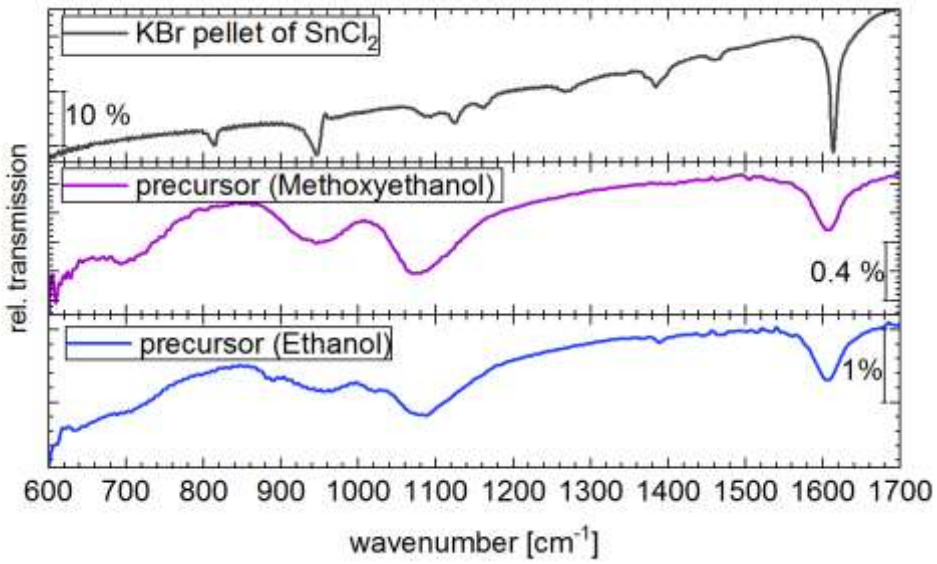

Figure S3. Infrared relative transmission spectra in the mid infrared range of precursor layers from a) methoxyethanol and b) ethanol as solvent. c) A potassium bromide (KBr) powder spectra of the $SnCl_2 \cdot 2\ H_2O$. The angle of incident of the p-polarized light was 7° towards the surface normal and the sample compartment was flushed with nitrogen during the measurement.

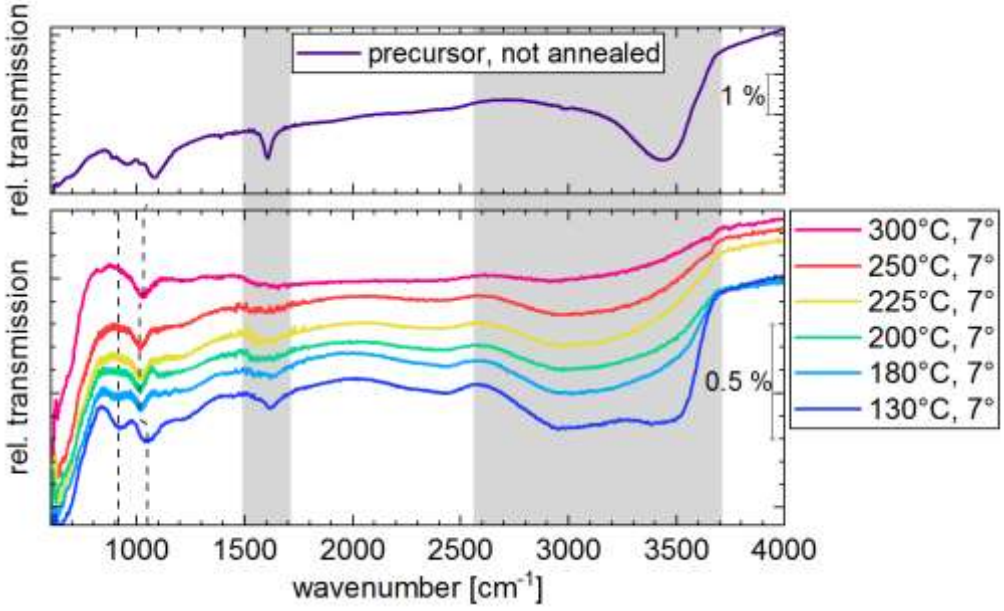

Figure S4. Infrared relative transmission spectra in the mid infrared range of tin oxide layer prepared from precursor solution with ethanol as solvent ($SnCl_2 \cdot 2\ H_2O$). The angle of incident of the p-polarized light was 7° towards the surface normal and the sample compartment was flushed with nitrogen during the measurement.

3. XPS

3.1. Comparison between ethanol and methoxyethanol for the precursor solution

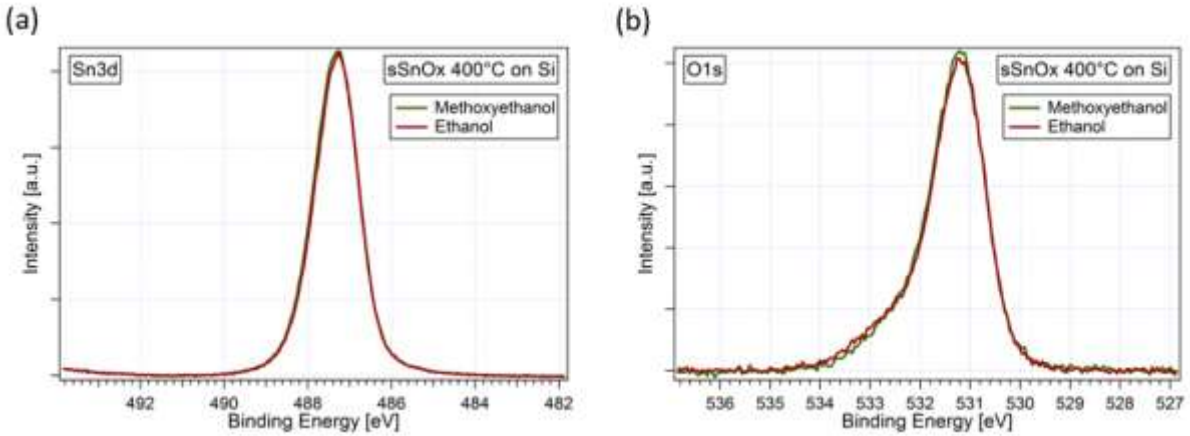

Figure S5. XPS detail spectra of (a) Sn 3d and (b) O 1s for tin oxide thin films annealed at 400 °C. The thin films were prepared from a precursor solution of $SnCl_2 \cdot 2\ H_2O$ in methoxyethanol (red) and ethanol (green). There is no obvious spectral change for the two different solvents.

3.2. Doping mechanism

To further illustrate the correlation between chlorine amount and the Fermi level position in the films, both the Sn $3d_{5/2}$ peak position (black) and the VBM (blue) are plotted against the chlorine amount (Figure 3e). An approximately linear relationship is obtained. This is reminiscent of a doping mechanism, in which the amount of dopant (here, chlorine) determines the Fermi level position in the film.

However, due to the large chlorine content in the present case, the observed Fermi level shift cannot be ascribed to doping in a classical sense, where a minimum quantity of dopant is sufficient to induce a significant Fermi level shift. The present case rather reminds on the doping mechanism in organic materials, where dopants are in large fractions and a charge transfer is expected to take place, although the exact mechanism is still under debate.[5,6] Even more, a similar phenomenon as the Fermi level shift in the present case has been observed for Cu-doped nickel oxide[7,8]. Here as well, the reason of the Fermi level shift was ascribed to a

charge transfer process between CuO and NiO clusters rather than a doping in a classical inorganic system. Therefore, also in the present case, a charge transfer mechanism is expected to cause the observed shift of the Fermi level. Still, the determination of the exact nature of this mechanism is subject of ongoing research.

3.3. Work function measurement

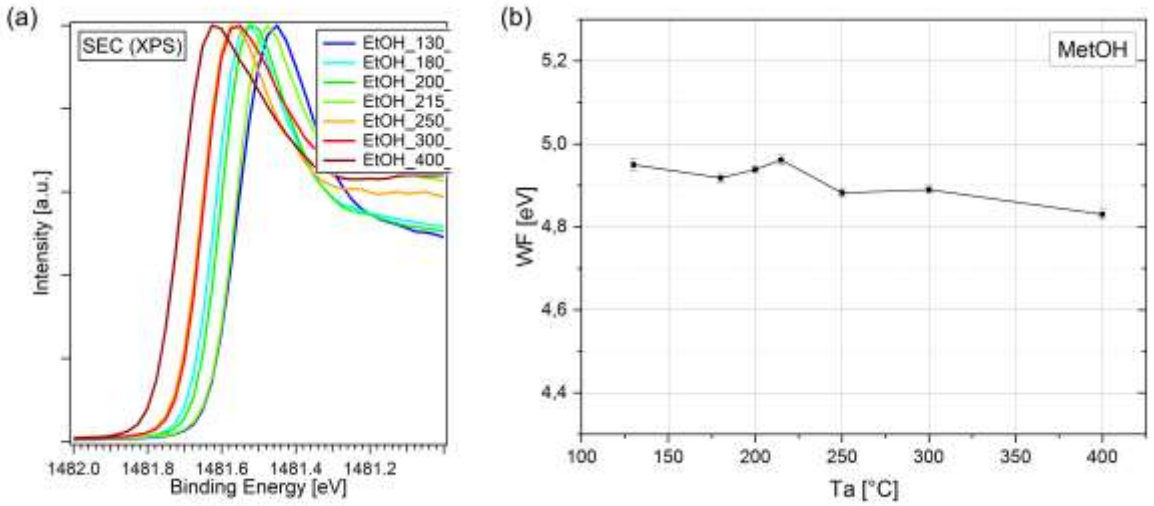

Figure S6. (a) Secondary electron cut-off of $sSnO_x$ thin films (ethanol precursor solution) annealed at different temperatures (130 °C (blue), 180 °C (light blue), 200 °C (green), 215 °C (yellow green), 250 °C (orange), 300 °C (red) and 400 °C (dark red)). (b) Work function of $sSnO_x$ thin films (methoxyethanol) as function of annealing temperature (Ta).

4. Perovskite Solar Cells

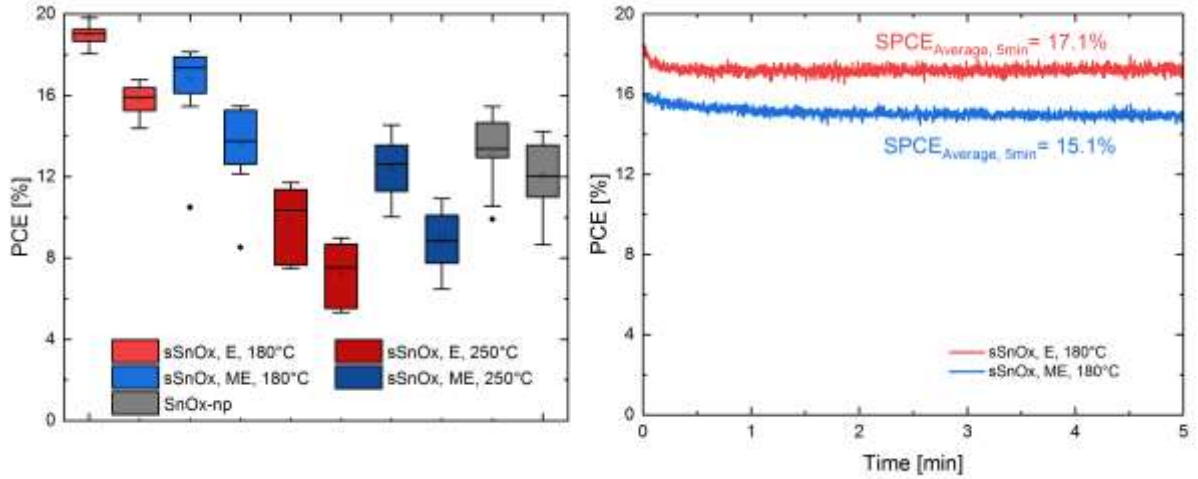

Figure S7. a) Performance of perovskite solar cells (fabricated as described in Experimental Section) in preliminary test batch with spin-coated solution processed tin oxide ($sSnO_x$) in ethanol (E) or methoxyethanol (ME) annealed at 180°C or 250°C. Devices with spin-coated tin oxide nanoparticles (SnO_x-np) have been added as comparison. b) Stabilized power conversion efficiency (SPCE) of test batch's champion devices measured by MPP-tracking. Note: The figure should only be used to identify general trends since such high overall efficiencies were not reproducibly achieved.

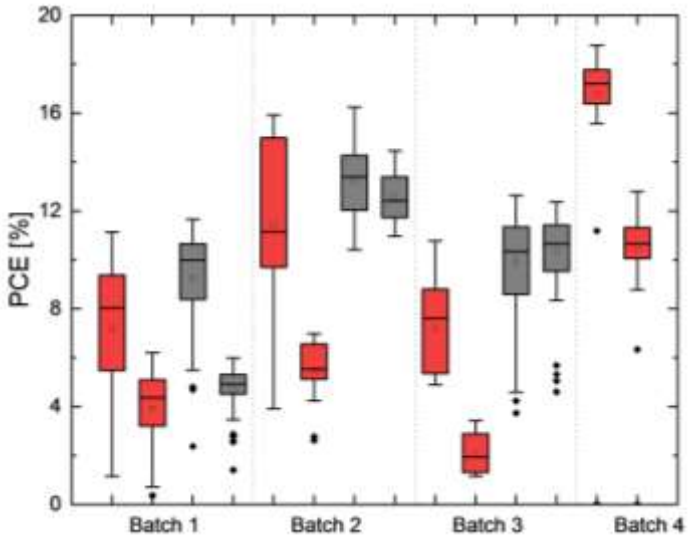

Figure S8. Distribution of power conversion efficiency perovskite solar cells with inkjet-printed precursor-based tin oxide (red) and spin-coated tin oxide nano particles as reference (grey). For batch 1 to 3 a tin oxide ink based on methoxyethanol, for batch 4 a modified ink based on a mixture of ethanol and butanol is used (see Experimental Section).

References

[1] W. Theiss, SCOUT - Software Package for Optical Spectroscopy. WTheiss Hardware and Software, 11875 E Elin Ranch Road, Tucson, AZ 85749, USA.

[2] S. Beck, D. Gerbert, T. Glaser, A. Pucci, *J. Phys. Chem. C* **2015**, *119*, 12545.

[3] F. Gervais, B. Piriou, *J. Phys. C Solid State Phys.* **1974**, *7*, 2374.

[4] F. Bréhat, B. Wyncke, J. M. Léonard, Y. Dusausoy, *Phys. Chem. Miner.* **1990**, *17*, 191.

[5] P. Reiser, *Dissertation*, Modifying and Controlling Diffusion Properties of Molecular Dopants in Organic Semiconductors, TU Darmstadt, November, **2019**.

[6] P. Reiser, L. Müller, V. Sivanesan, R. Lovrincic, S. Barlow, S. R. Marder, A. Pucci, W. Jaegermann, E. Mankel, S. Beck, *J. Phys. Chem. C.* **2018**, *122*, 14518.

[7] F. Ullrich, *Dissertation,* Photoelectron Spectroscopic Analysis of Solution-Processed Nickel Oxide: Surface Modification and Interfaces in Organic Solar Cells, TU Darmstadt, February, **2020**.

[8] S. Hietzschold, S. Hillebrandt, F. Ullrich, J. Bombsch, V. Rohnacher, S. Ma, W. Liu, A. Köhn, W. Jaegermann, A. Pucci, W. Kowalsky, E. Mankel, S. Beck, R. Lovrincic, *ACS Appl. Mater. Interfaces* **2017**, *9*, 39821.